First-order superfluid-to-Mott-insulator phase transitions in spinor condensates

J. Jiang, L. Zhao, S.-T. Wang, Z. Chen, T. Tang, L.-M. Duan, and Y. Liu

Phys. Rev. A **93**, 063607 — Published 7 June 2016

DOI: 10.1103/PhysRevA.93.063607

First-order superfluid to Mott-insulator phase transitions in spinor condensates

J. Jiang,[1,*] L. Zhao,[1,*] S.-T. Wang,[2] Z. Chen,[1] T. Tang,[1] L.-M. Duan,[2] and Y. Liu[1,†]

[1] *Department of Physics, Oklahoma State University, Stillwater, Oklahoma 74078, USA*
[2] *Department of Physics, University of Michigan, Ann Arbor, Michigan 48109, USA*

We observe evidence of first-order superfluid to Mott-insulator quantum phase transitions in a lattice-confined antiferromagnetic spinor Bose-Einstein condensate. The observed signatures include hysteresis effect, significant heatings across the phase transitions, and changes in spin populations due to the formation of spin singlets in the Mott-insulator phase. The nature of the phase transitions is found to strongly depend on the ratio of the quadratic Zeeman energy to the spin-dependent interaction. Our observations are qualitatively understood by the mean field theory, and in addition suggest tuning the quadratic Zeeman energy is a new approach to realize superfluid to Mott-insulator phase transitions.

PACS numbers: 67.85.Fg, 03.75.Kk, 03.75.Mn, 05.30.Rt

I. INTRODUCTION

A quantum phase transition from a superfluid (SF) to a Mott-insulator (MI) was realized in a scalar Bose-Einstein condensate (BEC) trapped by three-dimensional (3D) optical lattices around a decade ago [1]. Marking an important milestone, this achievement has stimulated tremendous efforts to apply highly controllable ultracold bosonic and fermionic systems in studying condensed matter models [2–6]. The SF-MI transitions have been confirmed in various scalar BEC systems via different techniques that can efficiently control the ratio of interatomic interactions to the mobility of atoms [1, 5–7]. One well-known approach to simultaneously enhance interatomic interactions and suppress atomic motion is by raising the depth of an optical lattice [1]. Another convenient method is to manipulate interactions with a magnetically tuned Feshbach resonance [7]. A third technique is to control the hopping energy of bosonic atoms by periodically shaking the lattice [6]. Spinor BECs, on the other hand, possess an additional spin degree of freedom, leading to a range of phenomena absent in scalar BECs [8–14]. One important prediction is the existence of first-order SF-MI phase transitions in lattice-trapped antiferromagnetic spinor BECs [2, 11, 13, 15–18]. In contrast, the phase transitions can only be second order in scalar BECs and ferromagnetic spinor BECs [2, 5, 17].

In this paper, SF-MI transitions are studied in sodium antiferromagnetic spinor BECs confined by cubic optical lattices. We observe hysteresis effect, changes in spin components, and substantial heating across the phase transitions. These indicate the existence of meta-stable states, the formation of spin singlets, and associated first-order transitions. In the ground state of the spinor BECs, the nature of SF-MI transitions is found to be determined by the competition between the quadratic Zeeman energy q_B and the spin-dependent interaction U_2. At low magnetic fields where U_2 dominates, signatures of first-order transitions are observed. In the opposite limit, the transitions appear to be second order and resemble those occurring in scalar BECs. These qualitative features are explained by our mean-field (MF) calculations. We also study the phase transitions with an initial meta-stable state and observe stronger heatings across all magnetic fields. Furthermore, our data indicate a new technique to realize SF-MI transitions is by varying q_B.

We describe lattice-trapped $F = 1$ spinor BECs with the Bose-Hubbard (BH) model [15, 19]. In the decoupling MF approximation, the Hamiltonian can be reduced to a site-independent form [12, 18, 20],

$$H_{\rm MF} = \frac{U_0}{2} n(n-1) + \frac{U_2}{2}(\vec{S}^2 - 2n) + q_B \sum_{m_F} m_F^2 n_{m_F} - \mu n - zJ \sum_{m_F} (\phi^*_{m_F} b_{m_F} + \phi_{m_F} b^\dagger_{m_F}) + zJ|\vec{\phi}|^2 \ . \quad (1)$$

U_0 is the spin-independent interaction, $n = \sum_{m_F} n_{m_F}$, and $n_{m_F} = b^\dagger_{m_F} b_{m_F}$ is the atom number per site of the m_F state. The vector order parameter is $\phi_{m_F} \equiv \langle b_{m_F} \rangle$, μ is the chemical potential, J is the nearest-neighbor hopping energy, z is the number of nearest neighbors, and $\vec{S}$ is the spin operator [21]. U_2 is positive (negative) in $F = 1$ antiferromagnetic (ferromagnetic) spinor BECs, e.g., $U_2 \simeq 0.04 U_0$ in ^{23}Na system [22]. With spatially uniform superfluids in equilibrium, one can assume ϕ_{m_F} to be real. $\phi_{m_F} = 0$ ($\neq 0$) in the MI (SF) phase.

An antiferromagnetic $F = 1$ spinor BEC of zero magnetization forms a polar superfluid in equilibrium with $\langle \vec{S} \rangle = 0$ [2, 22–24]. There are two types of polar superfluids: the longitudinal polar (LP) state with $(\phi_1, \phi_0, \phi_{-1}) = \sqrt{N_{\rm SF}}(0, 1, 0)$, and the transverse polar (TP) state with $(\phi_1, \phi_0, \phi_{-1}) = \sqrt{N_{\rm SF}/2}(1, 0, 1)$. Here $N_{\rm SF}$ is the number of condensed atoms per site. At zero q_B and the same $N_{\rm SF}$, TP and LP states are degenerate in energy. At $q_B > 0$, the MF ground state is always the LP state, but a meta-stable TP phase may exist [2, 24].

Our MF calculations show that q_B/U_2 is a key factor to understand the nature of SF-MI transitions in antiferromagnetic spinor BECs [25]. At low magnetic fields

* These authors contributed equally to this work.
† Electronic address: yingmei.liu@okstate.edu

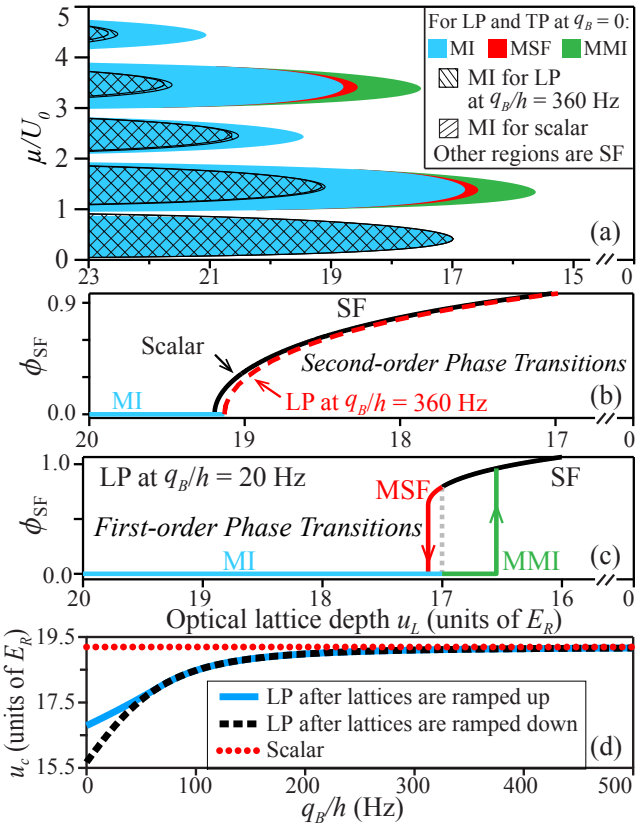

FIG. 1. (Color online) (a) MF phase diagrams derived from the BH model for scalar BECs [19], and the LP and TP sodium spinor BECs in cubic lattices (see Eq. (1)). The superfluid order parameter $\phi_{\rm SF}$ versus u_L at $\mu/U_0 = 1.4$ in (b) scalar and LP spinor BECs at $q_B/h = 360$ Hz, and (c) LP spinor BECs at $q_B/h = 20$ Hz. Here $|\phi_{\rm SF}|^2 = N_{\rm SF}$ and h is the Planck constant. (d) Predicted SF-MI transition point u_c versus q_B at $\mu/U_0 = 1.4$ (see Eq. (1)).

(where $0 \le q_B \lesssim U_2$), U_2 penalizes high-spin configurations and enlarges the Mott lobes for even number fillings as atoms can form spin singlets to minimize the energy. Meta-stable Mott-insulator (MMI) and meta-stable superfluid (MSF) phases emerge due to the spin barrier, and lead to first-order SF-MI transitions (see Figs. 1(a) and 1(c)) [15–18]. When 3D lattices are ramped up and down, hysteresis is expected across the phase transitions (i.e., different transition lattice depth u_c). In addition, when the system changes from a meta-stable phase to a stable phase (e.g., from MSF to MI), there will be a jump in the order parameter and the system energy, leading to unavoidable heating to the atoms. Hence, hysteresis, substantial heating, and the formation of spin singlets may be interpreted as signatures of first-order transitions. As q_B increases, the $m_F = 0$ state has lower energy than other m_F levels and U_2 becomes less relevant. When q_B becomes sufficiently larger than U_2 ($U_2/h \lesssim 80$ Hz in this work), the ground state phase diagram of antiferromagnetic spinor BECs reverts back to one that is similar to the scalar BH model with only second-order SF-MI transitions (see Fig. 1).

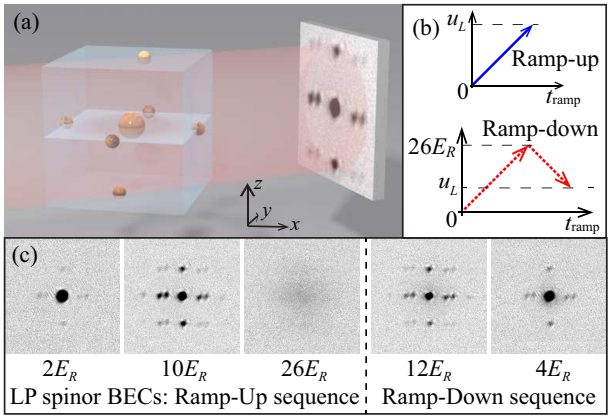

FIG. 2. (Color online) (a) Schematic of the reciprocal lattice and a TOF image taken after lattices are abruptly released. The area in red represents the imaging beam. (b) Two lattice ramp sequences used in this paper. (c) Interference patterns observed after we abruptly release LP spinor BECs at various final u_L followed by a 5.5-ms TOF at $q_B/h = 360$ Hz. The left (right) panel is taken after ramp-up (ramp-down) sequences. The field of view is 400 μm × 400 μm.

II. EXPERIMENTAL SETUP

Three different types of BECs (i.e., scalar BECs, LP and TP spinor BECs) are studied in this work. A scalar BEC containing up to 1.2×10^5 sodium atoms in the $|F = 1, m_F = -1\rangle$ state is created with an all-optical approach similar to Ref. [26]. A $F = 1$ spinor BEC of zero magnetization is then produced by imposing a resonant rf-pulse to the scalar BEC at a fixed q_B. Since the LP state (where $\rho_0 = 1$) is the mean-field ground state, it can be prepared by simply holding the spinor BEC for a sufficiently long time at high magnetic fields [24]. Here $\rho_{\rm m_F}$ is the fractional population of each m_F state. The TP state (where $\rho_{\pm1} = 0.5$) is generated via a different approach: we apply a resonant microwave pulse to transfer all $m_F = 0$ atoms in the $F = 1$ spinor BEC to the $F = 2$ state, and then blast away these $F = 2$ atoms with a resonant laser pulse. After quenching q_B to a desired value, we adiabatically load the BEC into a cubic optical lattice within time $t_{\rm ramp}$. This 3D lattice is constructed by three optical standing waves from a single-mode laser at 1064 nm, which results in a cubic periodic potential with a lattice spacing of 532 nm. All lattice beams are frequency-shifted by at least 20 MHz with respect to each other for eliminating cross interference among them. The calibration of optical lattice depth u_L is conducted via Kapitza-Dirac diffraction patterns and has an uncertainty of $\sim 15\%$. As shown in Fig. 2(b), lattices are linearly ramped up to a given u_L in a ramp-up sequence, while lattices are first adiabatically ramped up to $26E_R$ and then back down to a variable final u_L in a ramp-down sequence. Here $E_R = \hbar^2 k_L^2/(2M)$ is the recoil energy, M and $\hbar$ are respectively the atomic mass and the reduced Planck constant, and k_L is the lat-

tice wave-vector. We find that a ramp speed of $2E_R/\text{ms}$ is sufficient to satisfy the intraband adiabaticity condition and ensure $\geq 80\%$ of atoms remain in a scalar or a high-field LP spinor BEC after a ramp-down sequence to $2E_R$. We measure ρ_{m_F} with Stern-Gerlach imaging and microwave imaging after a certain time of flight (TOF).

III. FIRST-ORDER SUPERFLUID TO MOTT-INSULATOR PHASE TRANSITIONS

Distinct interference peaks can always be observed during ballistic expansion, after each BEC is abruptly released from a shallow lattice of $u_L \leq 10E_R$. As shown in the TOF images in Fig. 2, the six first-order diffracted peaks are symmetrically set apart from the central peak by a distance corresponding to a momentum of $2\hbar k_L$ along three orthogonal axes. These interference peaks may be considered as evidence for coherence associated with the SF phase. In fact, a larger visibility of interference patterns, a narrower width of the central peak, and a higher optical density (OD) of interference peaks have all been used as trustworthy evidence for improved phase coherence in atomic systems [1, 3, 5, 27].

TOF images in Fig. 2(c) show the loss and revival of the interference contrast in spinor BECs as cubic lattices are ramped up and down. A quantitative analysis of these TOF images demonstrates the interference peaks (i.e., coherence associated with the SF phase) change in a reversible manner with u_L (see Fig. 3). First, the interference patterns become more visible as lattices are made deeper, and reach their maximum OD around $10E_R$. This may be due to lattice-enhanced density modulation [3, 5, 27]. Second, when u_L is further increased and exceeds u_c, the interference peaks steadily smear out to a single broad peak indicating atoms completely lose phase coherence. We extract u_c in Fig. 3 from the intersection of two linear fits to the data of a given BEC. To confirm the system has undergone a SF-MI transition, we monitor lattice ramp-down sequences, because one characteristic of a MI state has proven to be a loss of phase coherence in deep lattices and a subsequent rapid revival of coherence as u_L is reduced [1, 3, 5]. The interference peaks of scalar and spinor BECs reversibly revive after ramp-down sequences, indicating atoms quickly recohere and return to SF states (see Fig. 3(b)).

Observations in Fig. 3 are qualitatively consistent with our MF calculations and suggest the existence of first-order SF-MI transitions under some circumstances. First, LP spinor BECs at high magnetic fields possess many properties (e.g., the peak OD) that are similar to those of scalar BECs. Their ramp-up and ramp-down curves are close to each other, while both have roughly symmetric transition points u_c. Similar phenomena were observed in ^{87}Rb and ^{6}Li systems, and have been considered as signatures of second-order SF-MI transitions [1, 3, 5]. Second, LP states at low magnetic fields and TP states at high fields apparently have smaller u_c for both ramp-up and ramp-down processes compared to scalar BECs, suggesting enlarged Mott lobes. Particularly, the ramp-down u_c for LP states at low fields is noticeably smaller than their ramp-up u_c, corroborating with the MF picture that hysteresis occurs across first-order phase transitions. Third, the recovered interference contrast is visibly different for various BECs after the ramp-down process (after SF-MI transitions). For scalar and high-field LP spinor BECs, nearly 75% of peak OD can be recovered in the interference peaks after ramp-down sequences. The slightly reduced interference contrast may be due to unaccounted heatings, which leads a small portion of atoms ($< 20\%$) to populate the Brillouin zone. In contrast, after we utilized quite a few techniques and optimized many parameters, the maximal recovered interference contrast of low-field LP states is only $\sim 40\%$ ($\sim 20\%$ for high-field TP states). We attribute this to unavoidable heatings across the first-order transitions as there is a jump in system energy between meta-stable states and stable states. Both hysteresis effect and significant heatings strongly suggest that first-order SF-MI transitions are realized in our experiment. Note, however, we do not see noticeable jumps in the observables as

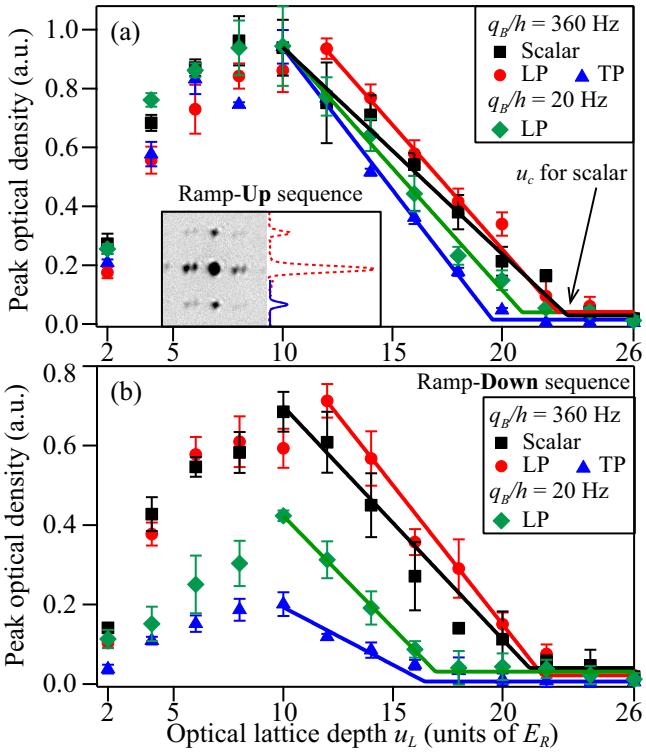

FIG. 3. (Color online) (a) Peak OD of interference peaks versus u_L after lattice ramp-up sequences. Markers are experimental data and lines are linear fits. We estimate u_c from the intersection of two linear fits to the data. The inset shows how we extract the peak OD from a TOF image (left). The dotted line in the right inset is a density profile of this TOF image through the central and one pair of interference peaks along the vertical direction, while the solid line is a bimodal fit to one side peak. (b) Similar to Panel(a) except that all data are taken after lattice ramp-down sequences.

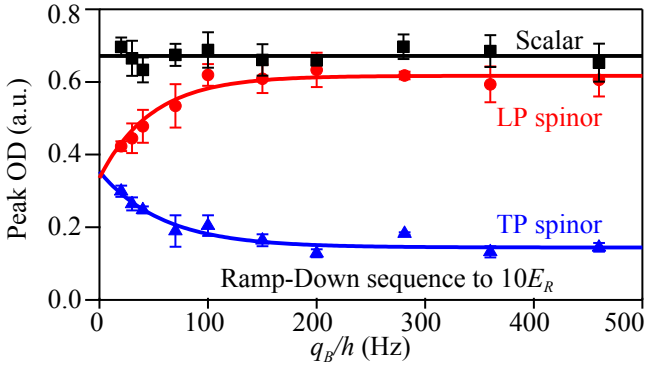

FIG. 4. (Color online) Peak OD of interference peaks versus q_B observed after lattice ramp-down sequences to $10E_R$. Markers are experimental data. Red and blue lines are exponential fits. The black line is a linear fit.

is typically associated with first-order transitions. This is likely due to the presence of even and odd atom fillings in inhomogeneous systems such as trapped BECs, although predicted first-order SF-MI transitions only exist for even occupancy number. Limited experimental resolutions may be another reason.

Our data in Fig. 3(b) also demonstrate that a new approach to realize SF-MI transitions is by ramping q_B at a fixed u_L. For example, when the final u_L in ramp-down sequences is set at a value between $17E_R$ and $21E_R$, atoms in LP spinor BECs can cross SF-MI transitions if q_B/h is sufficiently reduced (e.g., from 360 Hz to 20 Hz). This agrees with Fig. 1(d): u_c depends on q_B.

We then compare scalar and spinor BECs within a wide range of magnetic fields, $20\,\text{Hz} \le q_B/h \le 500\,\text{Hz}$, after identical lattice ramp sequences to $u_L = 10E_R$. We choose $10E_R$ because it is apparently the lattice depth around which we observe the maximum interference contrast, with negligible difference in scalar and spinor BECs after ramp-up sequences at all q_B. This is consistent with Fig. 1, which predicts all BECs studied in this work should be well in the SF phase at $10E_R$. However, the interference peak ODs show intriguing differences after ramp-down sequences to $10E_R$ (see Fig. 4): deviations from the maximal value appear for LP spinor BECs at low magnetic fields and the TP state at all positive q_B. We again attribute this to different amount of heatings across SF-MI transitions. Different extent of heatings may be produced due to different spin barriers as well as the amount of energy jump across the transitions. Hence, the maximum recovered OD is a good indicator for the appearance/disappearance of first-order SF-MI transitions. Notably, LP spinor BECs are found to behave very similarly to scalar BECs when $q_B \gg U_2$ (see Fig. 4). This observation is consistent with Fig. 1(d), in which the two MF curves for the LP state merge indicating that meta-stable states disappear and SF-MI transitions become second order when $q_B/h > 70\,\text{Hz}$. Furthermore, the difference between LP and TP spinor BECs appears to exponentially decrease as q_B approaches zero.

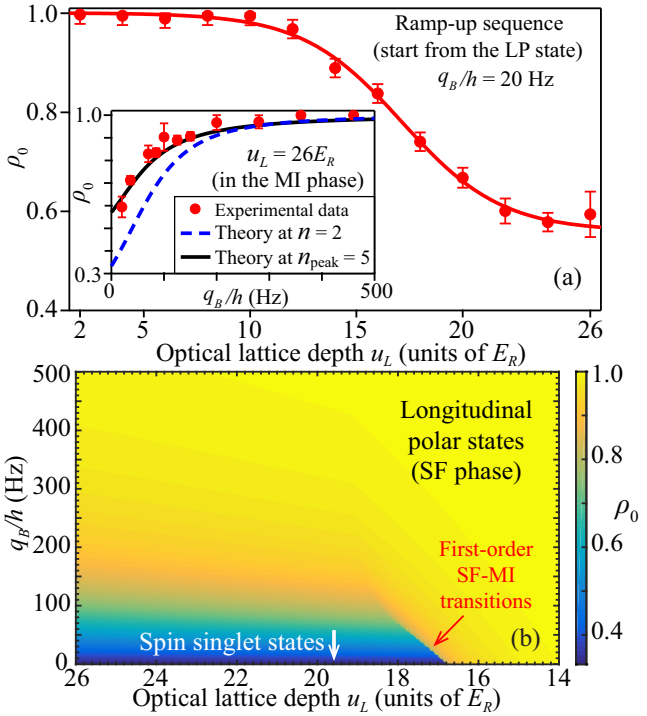

FIG. 5. (Color online) (a) Measured ρ_0 versus u_L after an initial LP spinor BEC undergoes ramp-up sequences to various final u_L at $q_B/h = 20\,\text{Hz}$. The solid line is a sigmoidal fit. Inset: Similar to the main figure except that we set q_B at various values, and the final u_L at $26E_R$ to ensure atoms enter into the MI phase. The dashed (solid) line represents the MF result for $n = 2$ ($n_{\text{peak}} = 5$). (b) Predicted ρ_0 in the ground state of antiferromagnetic spinor BECs at various u_L and q_B with $\mu/U_0 = 1.4$.

Exponential fits to the data verify that LP and TP spinor BECs should show the same behavior at $q_B = 0$.

Figure 5(a) shows the change in the fractional population ρ_0 as the lattice is ramped up, which provides another evidence that is consistent with first-order SF-MI transitions. In the MF picture, the first-order transition is related to the formation of spin singlets in the even lobe MI phase. For example, in the $n = 2$ MI lobe, the MI ground state $|\psi_g\rangle$ at zero q_B is the singlet state where $\rho_0 = \rho_{+1} = \rho_{-1} = 1/3$ [11, 13, 15–18], i.e., $|\psi_g(q_B = 0)\rangle = |S = 0, S_z = 0\rangle = \sqrt{\frac{2}{3}}|101\rangle - \sqrt{\frac{1}{3}}|020\rangle$ in the occupation basis of $|n_1, n_0, n_{-1}\rangle$. For $q_B > 0$, we diagonalize Eq. (1) in this occupation basis and find $|\psi_g\rangle = \dfrac{U_2 - 2q_B + \sqrt{4q_B^2 - 4q_BU_2 + 9U_2^2}}{2\sqrt{2}U_2}|101\rangle - |020\rangle$. This calculation result is shown in Fig. 5(b). A line at $u_L = 26E_R$ from Fig. 5(b) represents the result in the $n = 2$ Mott lobe, which is also highlighted as the theoretical $n = 2$ line in Fig. 5(a) inset. Two predictions can be derived from this MF calculation: ρ_0 drastically decreases as atoms cross the first-order transition (from SF to MI) and ρ_0 rises with q_B in the $n = 2$ Mott lobe.

Our observations shown in Fig. 5(a) may be the first experimental confirmation of these predictions: an initial LP state is found to sigmoidally evolve to a state consisting of all three m_F components as u_L is ramped up at low magnetic fields, with the measured ρ_0 sigmoidally decreasing from one in the SF phase to around 0.6 in the MI phase ($u_L \geq 22E_R$). In addition, in the MI phase, the measured ρ_0 rises with q_B, and approaches one at $q_B \gg U_2$ where the ground state phase diagram of antiferromagnetic spinor BECs resembles the scalar BH model with only second-order SF-MI transitions (see Fig. 5(a) inset). This observation can be well understood by the MF calculation (the $n_{\rm peak} = 5$ line in Fig. 5(a) inset). Note that the peak filling factor $n_{\rm peak}$ is five in our inhomogeneous system, the data in Fig. 5(a) thus represent an average of different atom fillings. In other words, the theoretical $n_{\rm peak} = 5$ line in Fig. 5(a) inset represents a weighted average of the MF predictions at five different n (i.e., $n = 1, 2, 3, 4, 5$) based on the atom density distribution in a harmonic trap. Good agreements between our data and the MF theory suggest that the observed substantial change in ρ_0 at very low fields may be mainly due to the formation of spin singlets in the even lobe MI phase (after atoms cross the first-order transitions).

IV. CONCLUSION

In conclusion, we have conducted the first experimental study on SF-MI transitions in lattice-confined sodium spinor BECs. We have observed hysteresis, significant heatings across the phase transitions, and the change in ρ_0 resulted from the formation of spin singlets in the MI phase. These observations strongly suggest first-order SF-MI transitions are realized in our system. Our data are understood by the MF theory, and also suggest SF-MI transitions can be realized by tuning q_B. Further studies are required to confirm more signatures of the first-order transitions, e.g., by precisely imaging Mott shells [4, 7].

V. ACKNOWLEDGMENTS

We thank the ARO and the NSF for financial support. STW and LMD are supported by the IARPA, the ARL, and the AFOSR MURI program. STW thanks Xiaopeng Li for helpful discussions.

[1] M. Greiner, O. Mandel, T. Esslinger, T. W. Hänsch, and I. Bloch, Nature **415**, 39 (2002).
[2] D. M. Stamper-Kurn and M. Ueda, Rev. Mod. Phys. **85**, 1191 (2013).
[3] J. K. Chin, D. E. Miller, Y. Liu, C. Stan, W. Setiawan, C. Sanner, K. Xu, and W. Ketterle, Nature **443**, 961 (2006).
[4] G. K. Campbell, J. Mun, M. Boyd, P. Medley, A. E. Leanhardt, L. G. Marcassa, D. E. Pritchard, and W. Ketterle, Science **313**, 649 (2006).
[5] I. Bloch, J. Dalibard, and W. Zwerger, Rev. Mod. Phys. **80**, 885 (2008).
[6] H. Lignier, C. Sias, D. Ciampini, Y. Singh, A. Zenesini, O. Morsch, and E. Arimondo, Phys. Rev. Lett. **99**, 220403 (2007).
[7] C. Chin, R. Grimm, P. Julienne, and E. Tiesinga, Rev. Mod. Phys. **82**, 1225 (2010).
[8] P. Windpassinger, and K. Sengstock, Rep. Prog. Phys. **76**, 086401 (2013).
[9] J. Heinze, S. Götze, J. S. Krauser, B. Hundt, N. Fläschner, D.-S. Lühmann, C. Becker, and K. Sengstock, Phys. Rev. Lett. **107**, 135303 (2011).
[10] P. Soltan-Panahi, J. Struck, P. Hauke, A. Bick, W. Plenkers, G. Meineke, C. Becker, P. Windpassinger, M. Lewenstein, and K. Sengstock, Nat. Phys. **7**, 434 (2011).
[11] S. S. Natu, J. H. Pixley, and S. Das Sarma, Phys. Rev. A **91**, 043620 (2015).
[12] K. W. Mahmud and E. Tiesinga, Phys. Rev. A **88**, 023602 (2013).
[13] G. G. Batrouni, V. G. Rousseau, and R. T. Scalettar, Phys. Rev. Lett. **102**, 140402 (2009).
[14] M. Shinozaki, S. Tsuchiya, S. Abe, T. Ozaki, and T. Nikuni, J. Low Temp. Phys. **175**, 236 (2014).
[15] E. Demler and F. Zhou, Phys. Rev. Lett. **88**, 163001 (2002); A. Imambekov, M. Lukin, and E. Demler, Phys. Rev. A **68**, 063602 (2003).
[16] K. V. Krutitsky, M. Timmer, and R. Graham, Phys. Rev. A **71**, 033623 (2005).
[17] T. Kimura, S. Tsuchiya, and S. Kurihara, Phys. Rev. Lett. **94**, 110403 (2005).
[18] D. Yamamoto, T. Ozaki, C. A. R. Sa de Melo, and I. Danshita, Phys. Rev. A **88**, 033624 (2013).
[19] M. P. A. Fisher, P. B. Weichman, G. Grinstein, and D. S. Fisher, Phys. Rev. B **40**, 546 (1989).
[20] R. V. Pai, K. Sheshadri, and R. Pandit, Phys. Rev. B **77**, 014503 (2008); A. Wagner, *Spinor condensates in optical superlattices*, Ph.D. thesis, University of Basel (2012).
[21] The linear Zeeman energy is ignored in Eq. (1), since it remains unchanged during collisional spin interconversions in $F = 1$ spinor BECs. The spin operators are given by $S_x = \frac{1}{\sqrt{2}}\left(b_0^\dagger b_1 + b_1^\dagger b_0 + b_{-1}^\dagger b_0 + b_0^\dagger b_{-1}\right)$, $S_y = \frac{i}{\sqrt{2}}\left(b_0^\dagger b_1 - b_1^\dagger b_0 + b_{-1}^\dagger b_0 - b_0^\dagger b_{-1}\right)$, $S_z = b_1^\dagger b_1 - b_{-1}^\dagger b_{-1}$.
[22] L. Zhao, J. Jiang, T. Tang, M. Webb, and Y. Liu, Phys. Rev. Lett. **114**, 225302 (2015).
[23] T.-L. Ho, Phys. Rev. Lett. **81**, 742 (1998); T. Ohmi and K. Machida, J. Phys. Soc. Jpn. **67**, 1822 (1998).
[24] J. Jiang, L. Zhao, M. Webb, and Y. Liu, Phys. Rev. A **90**, 023610 (2014).
[25] We solve Eq. (1) self-consistently by requiring $\phi_{m_F} = \langle b_{m_F} \rangle$ in the occupancy number n basis with a maximum of 15 atoms per site. Since the observed $n_{\rm peak}$ is five, the truncation errors are negligible.
[26] L. Zhao, J. Jiang, T. Tang, M. Webb, and Y. Liu, Phys. Rev. A **89**, 023608 (2014).
[27] K. Xu, Y. Liu, D. E. Miller, J. K. Chin, W. Setiawan and W. Ketterle, Phys. Rev. Lett. **96**, 180405 (2006).